

Elemental composition and material properties of radular teeth in the heterobranch snail *Gastropteron rubrum* (Mollusca, Gastropoda) foraging on hard organisms

Wencke Krings¹, Charlotte Neumann¹, Stanislav Gorb², Alexander Koehnsen¹, and Heike Wägele³

¹Universität Hamburg

²Kiel University

³Leibniz Institute for the Analysis of Biodiversity Change

May 3, 2023

Abstract

The molluscan feeding structure is the radula, a chitinous membrane with teeth, which are highly adapted to the food and the substrate. In Polyplacophora and Patellogastropoda, the handling of hard ingesta can be facilitated by high content of chemical compounds containing Fe or Si in the tooth cusps. Other taxa, however, possess teeth that are less mineralized, even though animals have to avoid structural failure or high wear during feeding as well. Here, we investigated the gastropod *Gastropteron rubrum*, feeding on hard Foraminifera, diatoms and Porifera. Tooth morphologies and wear were documented by scanning electron microscopy and their mechanical properties were tested by nanoindentation. We determined, that gradients of hardness and stiffness run along each tooth, decreasing from cusp to basis. We also found, that inner lateral teeth are harder and stiffer than the outer ones. These findings allowed us to propose hypotheses about the radula-ingesta interaction. In search for the origins of the gradients, teeth were visualized using confocal laser scanning microscopy, to determine the degree of tanning, and analyzed with energy-dispersive X-ray spectroscopy, to test the elemental composition. We found that the mechanical gradients probably have their origin in the degree of tanning, as the teeth did not contain high proportions of metals or other minerals. However, in the tooth surfaces, which interact with the ingesta, high Si and Ca content was determined, which is likely an adaptation to reduce wear.

Elemental composition and material properties of radular teeth in the heterobranch snail *Gastropteron rubrum* (Mollusca, Gastropoda) foraging on hard organisms

Wencke Krings^{1,2,3,4*}, Charlotte Neumann^{2,3}, Stanislav N. Gorb⁴, Alexander Koehnsen^{1,2}, Heike Wägele⁵,

¹ Department of Cariology, Endodontology and Periodontology, Universität Leipzig, Liebigstraße 12, 04103 Leipzig, Germany

² Department of Electron Microscopy, Institute of Cell and Systems Biology of Animals, Universität Hamburg, Martin-Luther-King-Platz 3, 20146 Hamburg, Germany

³ Department of Mammalogy and Palaeoanthropology, Leibniz Institute for the Analysis of Biodiversity Change, Martin-Luther-King-Platz 3, 20146 Hamburg, Germany

⁴ Department of Functional Morphology and Biomechanics, Zoological Institute, Christian-Albrechts-Universität zu Kiel, Am Botanischen Garten 1-9, 24118 Kiel, Germany

⁵ Department of Phylogenetics and Evolutionary Biology, Leibniz Institute for the Analysis of Biodiversity Change, Adenauerallee 160, 53113 Bonn, Germany

*corresponding author: wencke.krings@uni-hamburg.de

Abstract

The molluscan feeding structure is the radula, a chitinous membrane with teeth, which are highly adapted to the food and the substrate. In Polyplacophora and Patellogastropoda, the handling of hard ingesta can be facilitated by high content of chemical compounds containing Fe or Si in the tooth cusps. Other taxa, however, possess teeth that are less mineralized, even though animals have to avoid structural failure or high wear during feeding as well. Here, we investigated the gastropod *Gastropteron rubrum*, feeding on hard Foraminifera, diatoms and Porifera. Tooth morphologies and wear were documented by scanning electron microscopy and their mechanical properties were tested by nanoindentation. We determined, that gradients of hard- and stiffness run along each tooth, decreasing from cusp to basis. We also found, that inner lateral teeth are harder and stiffer than the outer ones. These findings allowed us to propose hypotheses about the radula-ingesta interaction. In search for the origins of the gradients, teeth were visualized using confocal laser scanning microscopy, to determine the degree of tanning, and analyzed with energy-dispersive X-ray spectroscopy, to test the elemental composition. We found that the mechanical gradients probably have their origin in the degree of tanning, as the teeth did not contain high proportions of metals or other minerals. However, in the tooth surfaces, which interact with the ingesta, high Si and Ca content was determined, which is likely an adaptation to reduce wear.

Keywords

Mollusca, elemental composition, biomineralization, feeding, mechanical properties

Introduction

Feeding structures can be highly adapted to the preferred ingesta (i.e., food, particles on the food, substrate that the food is attached to). In molluscs, the radula is the structure that processes food/ingesta intake. It is a unique molluscan development and consists of a chitin membrane with embedded rows of teeth. The tooth morphology and the arrangement of teeth on the membrane can relate to the ingesta source (e.g., Solem, 1972, 1974; Steneck & Watling, 1982; Hawkins et al., 1989; Padilla, 2003; Ukmar-Godec et al., 2015; Krings et al., 2021b, 2021c, 2021d).

Even though the radula is constantly renewed by secretion in the posterior radular region (the “radular sac”) by over- and underlain epithelia (Runham, 1963; Runham & Isarankura, 1966; Mackenstedt & Märkel, 1987; Vortsepneva et al., 2022), the radular material properties are adapted during formation to reduce wear and/or structural failure induced by the specific ingesta source.

Structural failure can be reduced by the presence of mechanical property gradients (i.e., of the Young’s modulus) along each tooth. In polyplacophorans, limpets, or some gastropod taxa (e.g., some members of the Paludomidae and Nudibranchia), the radula needs to transfer high forces to solid surfaces (e.g., rocks) by scratching action or to hard structures of the prey (e.g., sponge spiculae) by piercing action. Here, each tooth shows pronounced gradients with the cusp as the hardest and stiffest region, followed by the stylus and finally the basis, as the softest and most flexible region (van der Wal et al., 1999; Weaver et al., 2010; Lu & Barber, 2012; Herrera et al., 2015; Krings et al., 2019, 2022c, 2022d, 2023; Pohl et al., 2020; Gorb & Krings, 2021). This allows teeth to bend and to either gain support from the next row of teeth, which redistributes the stress, or to deform and adjust to the prey item to avoid structural damage. These mechanical property gradients have their origin in the degree of tanning, the content of inorganics, the regional water content or the chitin fiber arrangement (e.g., Brooker & Shaw, 2012; Faivre & Ukmar-Godec, 2015; Joester & Brooker, 2016; Krings et al., 2021b, 2022d).

With regard to abrasion resistance, some taxa, like Polyplacophora and Patellogastropoda, incorporate high proportions of iron and silicon into their very thick tooth leading edge (i.e., the surface of the tooth that interacts directly with the ingesta) resulting in hard tooth cusps as adaptation to feeding on algae growing on stone (e.g. van der Wal et al., 1999; Wealthall et al., 2005; Shaw et al., 2009a, 2009b, 2010; Weaver et al., 2010; Saunders et al., 2011; Han et al., 2011; Lu & Barber, 2012; Wang et al., 2014; Barber et al., 2015;

Krings et al., 2022c). High inorganic contents such as Ca or Si were also found on the leading edges (“leading surfaces”) of other gastropod taxa (e.g., some Paludomidae foraging on algae also growing on rock, and Nudibranchia foraging on Porifera as well. However, the coating was very thin in comparison to the leading edge of Polyplacophora, suggesting that these teeth resemble highly functional lightweight structures (Krings et al., 2022a, 2023). Teeth that come in contact with abrasive particles, like sand, were found to contain a thin layer with high content of Ca on all tooth surfaces, presumably to prevent high wear (Krings & Gorb, 2023a).

In this context, we here aim at unravelling the functional principles that reflect adaptation to the ingesta source in the radular teeth of the gastropod *Gastropteron rubrum* (Rafinesque, 1814) (Heterobranchia, Euopisthobranchia), which forages on Foraminifera (DeLaHoz et al., 2018). Members of these single celled protists have a calciumcarbonate skeleton and thus represent a hard and abrasive ingesta. This is the first tooth analysis of a gastropod that mainly preys on this kind of food. First, the stomach content of the sea slug was documented under scanning-electron-microscopy (SEM) to gain insight into the food composition in detail. Then, the teeth were carefully documented unravelling the wear at the tooth cusps. The mechanical properties of the teeth were tested using nanoindentation technique to get insights on the functional adaptations of the radular apparatus. In the search for the origins of the mechanical properties in the teeth, we also investigated the material composition. The degree of tanning of the teeth was visualized using confocal laser scanning microscopy (CLSM), and the elemental composition were analyzed with energy-dispersive X-ray spectroscopy (EDS, EDX).

Material & methods

Specimens and preparation

Individuals of *Gastropteron rubrum* were collected by Yvonne Grzybowski at Els Capets, Costa Brava, Spain, in November 2004, and fixed in 96% EtOH. Eight adult specimens were dissected for this study.

Scanning electron microscopy (SEM) and 3D visualization

For documentation of morphology using SEM, three radulae were carefully extracted and cleaned by a short ultrasonic bath in 70% EtOH. Subsequently they were mounted on SEM specimen holders by double-sided adhesive carbon tape and sputter-coated with platinum (5 nm layer). For visualization, we used a SEM Zeiss LEO 1525 (One Zeiss Drive, Thornwood, NY, USA). Only mature teeth from the working zone, which can be identified by lack of covering epithelia, were studied. To document the wear on the teeth, radulae were rewetted by 70% EtOH afterwards, cleaned by a short ultrasonic bath, rearranged on SEM sample holders and visualized again in the SEM. Nomenclature of teeth was adapted from (Ong et al., 2017).

For the 3D visualization, mature radular teeth of the working zone of two radulae were extracted manually with forceps. Each tooth was mounted on SEM specimen holders by double-sided adhesive carbon tape, sputter-coated with platinum (5 nm layer), and visualized under the SEM from all sides. Using the 3D software Blender v2.83 (Blender Foundation), the teeth were then modelled by hand always comparing the 3D visualization with the SEM images taken from different sides (see also protocol in Krings et al., 2020, 2021e). In the same manner, the position and embedment of the teeth within the membrane were reconstructed.

Ingesta analyses

For ingesta analyses, the intestines of four specimens were opened and the particles carefully extracted by tweezers. We differentiated between ingesta in the proximal and the distal part of the intestine.

Confocal laser scanning microscope (CLSM)

To document the autofluorescence of the tooth material, two clean radulae and some individual mature teeth were arranged on object glass slides, following the procedure of Michels & Gorb (2012). Each radula was surrounded by a stack of reinforcement rings. The rings were filled with glycerin (greater than or equal to 99.5%, free of water, Carl Roth GmbH & Co. KG, Karlsruhe, Germany) and subsequently covered by a glass

cover slip. Following the protocol of Krings et al. (2022d, 2023), samples were visualized employing a Zeiss LSM 700 confocal laser scanning microscope (Carl Zeiss Microscopy GmbH, Jena, Germany). Four stable solid-state lasers with wavelengths of 405 nm, 488 nm, 555 nm, and 639 nm were used. Bandpass or longpass emission filters (420–480 nm, greater than or equal to 490 nm, greater than or equal to 560 nm, or greater than or equal to 640 nm) were applied. After scanning, images of autofluorescence were superimposed (with maximum intensity projection) using the software Zeiss Efficient Navigation (Zen) (Carl Zeiss MicroImaging GmbH). Finally, the color blue was assigned to the autofluorescence signal received from the laser with wavelength 405 nm, green to 488 nm, red (50% saturation) to 555 nm and red (50% saturation) to 639 nm.

Energy dispersive X-ray spectroscopy (EDX)

For analysis of the elemental composition, three cleaned radulae (ultrasonic bath for 20 seconds) were attached to glass object slides by double-sided adhesive tape, following our previous protocol (Krings et al., 2022a, 2022c, 2023). Then, each radula was surrounded by a small metallic ring. Afterwards the ring was filled with epoxy resin (Reckli Epoxy WST, RECKLI GmbH, Herne, Germany) to cover the radula completely. After polymerization, lasting for three days at room temperature, glass object slides and adhesive tape were removed. Samples were polished with sandpapers of different roughness until teeth were on display and smoothed with aluminum oxide polishing powder suspension of 0.3 μm grain size (PRESI GmbH, Hagen, Germany) on a polishing machine (Minitex 233/333, PRESI GmbH, Hagen, Germany) to receive a plain smooth surface. The embedding and smoothing prevent artefacts such as electron scattering during EDX analysis. Embedded samples were subsequently cleaned in an ultrasonic bath for five minutes, then mounted on SEM sample holders and sputter-coated with platinum (5 nm layer). Elemental composition was determined with the SEM Zeiss LEO 1525 equipped with an Octane Silicon Drift Detector (SDD) (micro analyses system TEAM, EDAX Inc., New Jersey, USA). For each sample, the same settings were used (i.e. an acceleration voltage of 20 kV, working distance, lens opening, etc.). Before analysis, the detector was calibrated with copper.

Small areas (no mapping) were analyzed to receive the data. Following elements were detected and their proportions measured.: H (hydrogen), C (carbon), N (nitrogen), O (oxygen), Pt (platinum), Al (aluminum), Ca (calcium), Cl (chlorine), Cu (copper), Fe (iron), K (potassium), Mg (magnesium), Na (sodium), P (phosphorus), S (sulphur), Si (silicon), and Zn (zinc). Some elements were not discussed as they are either the elemental basis of chitin and proteins (H, C, N, O), the coating (Pt), or the polishing powder (Al, O). For test purposes, we also performed 10 EDX tests on the epoxy to identify putative pollution due to the mechanical application, embedding or polishing. We could not detect Si (which is part of the sandpaper), or any other elements, that we further discuss as Ae (Ca, Cl, Cu, Fe, K, Mg, P+Pt, S, Si, Zn), in the resin. Their presence is therefore considered part of the teeth.

The single peak of P overlaps with one of Pt. Due of this, the software could not discriminate between these two elements and P content could not be reliably determined. Therefore, P and Pt are discussed together (P+Pt). We, however, measured 20 areas of pure epoxy to receive values on their Pt content (mean \pm SD; 0.15 ± 0.02 atomic %) to further estimate the proportions of P in the teeth.

We tested the inner tooth structure by EDX and the thin outer layer (“surface”) of the teeth (500–1000 nm thickness), which covers the inner tooth structure. We did not detect high content of elements in the inner structure and no differences in the distribution there. We thus decided to summarize the point measurements of the inner structure. With regard to the surfaces, we could determine variations in the distribution of elements and thus differentiated between the tooth basis, the bulges, the basal region of the stylus (stylus, basis), the terminal region of the stylus (stylus, terminal), the cusps and the sides (see Figures 1 and 2 for nomenclature). 474 point measurements on 180 mature teeth were conducted: 204 on 70 inner laterals (of which 70 on the inner tooth structure and 134 on the surface); 56 (22 on the inner tooth structure and 34 on the surface) on 22 outer laterals A, B, C; 54 (22 on the inner tooth structure and 32 on the surface) on 22 outer laterals D; 48 (22 on the inner tooth structure and 26 on the surface) on 22 outer laterals E.

Nanoindentation

To test the mechanical properties, nanoindentation experiments were performed on three additional radulae (for detailed protocol see Krings et al., 2022c, 2022d, 2023; Gorb & Krings, 2021). Radulae were arranged on glass object slides and surrounded by a small metallic ring. Afterward, each ring was filled with epoxy resin, which covered the radula completely. After polymerization, samples were polished with sandpapers until tooth sections were on display (see Supplementary Figure 1), and smoothed with aluminum oxide polishing powder suspension on a polishing machine. Samples were cleaned in an ultrasonic bath for five minutes. A nanoindenter SA2 (MTS Nano Instruments, Oak Ridge, Tennessee, USA) equipped with a Berkovich indenter tip and a dynamic contact module (DCM) head was employed. Hardness (H) and Young's modulus (E) were determined from force-distance curves by applying the continuous stiffness mode. All tests were performed under normal room conditions (relative humidity 28–30%, temperature 22–24 °C) and each indent and corresponding curve were both manually controlled. After this, samples were smoothed and polished until the next target localities were on display.

Overall, the inner structure of each tooth was tested at five localities to receive data on mechanical property gradients within each tooth. E and H were determined at penetration depths of 500–1000 nm. For each site indented, we received ~60 values obtained at different indentation depths, which were averaged to receive one H and one E mean value per indent. 413 localities were overall tested: 118 on the inner lateral, 59 on the outer lateral A, outer lateral B, outer lateral C, outer lateral D and outer lateral E respectively.

Statistical analyses

All statistical analyses were performed with JMP Pro, Version 14 (SAS Institute Inc., Cary, NC, 1989–2007). Mean values and standard deviations were calculated and Shapiro-Wilk-W-tests for testing of normality was conducted. As the data was non-normally distributed, a Kruskal-Wallis/Wilcoxon test, followed by pairwise comparison with Wilcoxon method, was carried out.

Results

Morphology and wear of teeth

Individuals of *Gastropteron rubrum* possessed per row one prominent inner lateral tooth, followed by five outer laterals to each side of the radula (see Figures 1A and 2A–F). The size of these outer laterals decreased towards the margin of the radula. A central tooth was missing and the prominent inner laterals were separated by a groove. Each inner lateral contained about 10 small denticles on the medial side and a bulge on the lateral side. Each outer lateral possessed one large cusp (tip).

Using SEM, we investigated signs of wear for each tooth type. On the inner laterals, spalling (Figures 1D, 1E and G) and scratches (Figure 1C) on the cusps and the denticles were found (see Figure 1A–E); in some cases, structural loss was rather high on these regions (Figure 1G). In contrast, we did not find scratches or spalling on the outer laterals (Fig. 1F); the degree of wear decreased in the outer laterals lying towards the margin of the radula.

Ingesta analyses

Analyses of the intestine revealed, that *Gastropteron rubrum* takes in sand particles, Foraminifera and diatoms (Figure 3D–G). However, spicules of the tylostyle type were also found, which indicate Heteroscleromorpha sponges, like Axinellida, Biemnida, Merliida, Polymastiida, Clionaida, Tethyida and Suberitida, as additional food (see Morrow & Cárdenas, 2015) (Figure 3A–C). The prey structures extracted from the distal region of the intestine (see Figure 3G) were more brittle and fractured than those from the proximal region of the intestine (compare with Figure 3D).

Autofluorescence signals

All cusps and the denticles from inner lateral teeth emitted a strong green autofluorescence signal on their anterior and posterior surfaces, i.e., they emitted a strong signal after excitement with the 488 nm laser. The cusps' lateral surfaces, the tooth styli and bases appeared rather red- to yellow-brown, i.e., emitted a strong signal after excitement with the lasers of 555 and 639 nm wavelength (see Figure 4). The bulges and

bases of the teeth exhibited a strong blue signal, i.e., emitted a strong signal after excitement with the 405 nm laser).

Elemental analysis by EDX

EDX can determine the elements present, but not the bonding conditions. We detected Ca, Cl, Cu, Fe, K, Mg, P+Pt, S, Si and Zn in the teeth (see Figure 5). The content of each individual element, except Fe, showed highly significant differences between the inner structure and the surface (results from Wilcoxon-test: $p < .0001^*$, for p-values see Supplementary Table 1).

In the inner tooth structure, the following proportions were found (sorted from high to low mean content): P+Pt (mean \pm standard deviation: 0.56 ± 0.26 atomic %), Fe (0.53 ± 0.35), Ca (0.47 ± 0.23), S (0.34 ± 0.12), Mg (0.26 ± 0.09), Zn (0.06 ± 0.03), Cu (0.05 ± 0.04), Si (0.04 ± 0.13), Cl (0.03 ± 0.03) and K (0.03 ± 0.02). All lateral teeth showed a rather small proportion of these elements in the inner tooth structure, compared to the surface (see below) (see Supplementary Table 2 for elemental content in the inner structure of the different teeth). Between the tooth types, we could not detect significant differences by pairwise comparison for the individual elemental content (see Supplementary Table 3 for p-values).

In the surface layer, the following proportions were detected (sorted from high to low mean content): Si (mean \pm standard deviation: 5.79 ± 6.40 atomic %), Ca (2.28 ± 2.28), P+Pt (0.85 ± 0.60), S (0.67 ± 0.30), Fe (0.60 ± 0.72), Mg (0.34 ± 0.20), Cu (0.14 ± 0.11), Zn (0.12 ± 0.08), Cl (0.08 ± 0.08) and K (0.05 ± 0.03). In each tooth, especially Si and Ca were present in larger proportions in comparison to the other elements (see Supplementary Table 2 for elemental content of the surfaces).

When the results from the outer tooth surface were sorted according to the tooth region (see Figure 2 for nomenclature and 6 for results), we found that the cusps contained highest content of all elements (Ae), followed by the styli (terminal), the styli (bases), the sides, the bases, and finally the bulges with the lowest content of Ae (see Supplementary Table 4). This gradient in Ae is primarily due to the content and distribution of Si (at cusps, mean \pm standard deviation: 16.24 ± 2.76 atomic %; at bulges: 0.27 ± 0.14) and Ca (at cusps: 5.56 ± 2.01 ; at bulges: 0.05 ± 0.05). But the Fe content, which was present in lower proportions, probably also contributes to the gradient, (at cusps: 1.26 ± 0.75 ; at bulges: 0.09 ± 0.07) (see Supplementary Table 4 for elemental content). The decrease of Si, Ca and Fe from tip to base of the teeth were found in each tooth type (see Supplementary Table 5 for elemental content of the different teeth and their regions) and differences when comparing the various regions of each tooth were highly significant (see Supplementary Table 6 for p-values). For the distribution of Cl, Cu, K, Mg, P+Pt, S and Zn no clear gradient could be detected, even though most regions differed highly significantly as determined by pairwise comparison (see Supplementary Table 6 for p-values). These elements were present in rather small proportions in each tooth (mean is < 1 atomic %; see Supplementary Tables 2 and 4). When comparing the different teeth, we could not determine clear differences between them (see Supplementary Figure 2). In most cases we detected highly significant differences between the individual regions of the surface when comparing the different teeth by pairwise comparison for Si, Ca and Fe (see Supplementary Tables 3 for p-values).

Mechanical properties

The hardness (H) describes the resistance to local plastic deformation induced by abrasion or indentation. The Young's modulus (E) is the measure of the stiffness of a solid material and describes the relationship between tensile stress and axial strain.

In every tooth, the cusp (E mean values range between 10.27 and 15.95 GPa; H mean values range between 0.58 and 0.85 GPa) was always the stiffest and hardest region, followed by the terminal stylus (E=8.51–14.18 GPa; H=0.47–0.77 GPa), the basis of the stylus (E=7.58–12.09 GPa; H=0.41–0.64 GPa), the basis (E=2.64–4.23 GPa; H=0.14–0.23 GPa) and finally the bulge as the softest and most flexible region (E=1.75–1.84 GPa; H=0.09–0.10 GPa). The parts of the inner laterals were harder and stiffer, followed by the outer laterals A, B, C, D and finally E with the softest and most flexible parts (see Figure 7 and Supplementary Table 7 for all values).

Pairwise comparison by Wilcoxon method revealed, that the regions within each tooth showed highly significant differences ($p < 0.0001^*$; see Supplementary Tables 8 and 9 for all p-values). Most regions were also highly significantly different, when they were compared between the teeth (mostly $p < 0.0001^*$; see Supplementary Tables 8 and 9 for all p-values).

Despite the differences of E and H values along the various regions of each tooth and between teeth, the two values always exhibited a very high positive correlation ($r = 0.99$, $p < 0.0001^*$) within a specific locality.

Relationship between autofluorescence, elemental composition and mechanical properties

The regions of the teeth appearing green under CLSM (i.e., emitted a strong signal after excitement with the 488 nm laser) contained high proportions of Si and Ca. The sides of the stylus and the bases appeared red- to yellow-brown (i.e., emitted a strong signal after excitement with the lasers of 555 and 639 nm wavelength); here no high content of Ca and Si were detected. The bulges appeared blue (i.e., emitted a strong signal after excitement with the lasers of 405 nm wavelength); these regions contained no high content of the targeted elements and were the softest and most flexible tooth parts. We could not determine relationships between the elemental content of the inner tooth structure and the mechanical property values.

Discussion

Mechanical behaviour and foraging

The mechanical properties of materials directly contribute to the mechanical behaviour of structures. The Young's modulus (E) relates to the ability of a structure to transmit force (Bendsøe & Kikuchi, 1988; Bendsøe, 1989, 1995; Dumont et al., 2009) and its resistance to failure, as well as the structures' mechanical behaviour while puncturing (e.g., Freeman & Lemen, 2007; for review on puncture mechanics see Anderson, 2018). The hardness (H) is the measure of the resistance to local plastic deformation induced by indentation or abrasion.

Some gastropod species (i.e., paludomid taxa) feeding on soft ingesta (i.e., algae growing on soft substrate like sand or mud) possess soft and more flexible teeth (E [?] 8 GPa, H [?] 1 GPa) without clear and pronounced gradients in mechanical properties from the tooth basis across the stylus to the cusp (Gorb & Krings, 2021). These teeth are probably not capable of transferring high forces without structural failure, but possess an increased ability to deform, bend, and twist, which reduces the risk of breaking (Krings et al., 2021b, 2021c). Since all teeth within one row have similar mechanical properties, they probably also have a similar function ("monofunctional radula"; see Krings, 2020; Gorb & Krings, 2021).

Species foraging on the solid ingesta (members of Paludomidae foraging on algae covering rocks, Patellogastropoda, Fissurellidae, Polyplacophora) or have some interactions with hard ingesta (the nudibranch gastropods *Felimare picta* and *Doris pseudoargus* feeding on Porifera with hard spiculae) possess harder and stiffer teeth reducing wear and structural failure. Each tooth shows pronounced gradients in both H and E: the cusp (especially the leading surface) is the hardest and stiffest part, followed by the stylus, and finally the basis with the softest and most flexible part (Weaver et al., 2010; Lu & Barber, 2012; Grunefelder et al., 2014; Barber et al., 2015; Ukmar-Godec et al., 2017; Krings et al., 2019, 2022c, 2022d, 2023; Gorb & Krings, 2021). In the above mentioned taxa, the tooth cusps puncture the ingesta or scratch across solid surfaces with the possible formation of local stress at the cusps, but without high degrees of wear or structural failure. The softer and more flexible stylus, together with the basis, provides flexibility and act as shock absorber against mechanical impacts (Herrera et al., 2015; Krings et al., 2019, 2022c, 2022d, 2023; Pohl et al., 2020; Gorb & Krings, 2021).

The dominant teeth of the so far investigated Polyplacophora are characterized by a very high inorganic content and the E values range from 30 to 130 GPa and H values from 4 to 12 GPa (Weaver et al., 2010; Grunefelder et al., 2014; Krings et al., 2022c). In the highly mineralized dominant teeth of *Patella vulgata* (Patellogastropoda), E values from 52 to 150 GPa and H values of 3 to 7 GPa were detected (Lu & Barber, 2012; Barber et al., 2015). Less mineralized teeth are softer and more flexible: in the vetigastropod *Megathura crenulata* (Fissurellidae) E values of 16 GPa were determined (Ukmar-Godec et al., 2017).

In the two investigated nudibranch species, where the inner structure of teeth also contained low inorganic content, E_{\max} values of 15 GPa and H_{\max} values of 0.9 GPa were found (Krings et al., 2023). Their thin leading surfaces were however significantly harder ($H_{\max} = 2.3$ GPa) and stiffer ($E_{\max} = 45$ GPa) than the inner structure, due to high proportions of Si or Ca. The unmineralized teeth of paludomid gastropods foraging from solid surfaces were even softer and more flexible in comparison to the inner structure of the nudibranch taxa ($H = \sim 0.4$ GPa and $E = \sim 8$ GPa; see Gorb & Krings, 2021). However, here the neighboring teeth could interlock when loaded, leading to stress redistribution when in contact with the ingesta. This mechanical behaviour is prospered by the arrangement and geometry of teeth, the water-content and the material properties which enables the bending capacity (Solem, 1972; Hickman, 1980, 1984; Morris & Hickman, 1981; Padilla, 2003; Ukmar-Godec et al., 2015; Herrera et al., 2015; Montroni et al., 2019; Krings et al., 2020, 2021b, 2021c, 2021d, 2021e; Krings & Gorb, 2021).

In some solid substrate feeders (i.e., the nudibranch gastropods *Felimare picta* and *Doris pseudoargus*), the different teeth of each row had similar mechanical properties. Here, teeth probably also had similar functions (“monofunctional radula”; Krings et al., 2023). However, in other taxa, there were pronounced gradients within each transversal tooth row present, i.e. different tooth types had different mechanical properties. E.g., in some paludomid gastropods, the central teeth were the stiffest and hardest elements, followed by the lateral, and finally the marginal teeth (Krings et al., 2019, 2022d; Gorb & Krings, 2021). The central and lateral teeth are probably capable of loosening algae from rocks, whereas the marginal teeth rather collect loosened food particles in a complex motion of the buccal mass afterwards. Since teeth of one row probably had different functions, this type of radula was previously termed “multifunctional radula” (see Krings, 2020; Gorb & Krings, 2021).

The teeth of *Gastropteron rubrum* show mechanical properties that were comparable to Nudibranchia teeth. In *G. rubrum*, the large inner laterals are harder and stiffer than the smaller outer laterals, with the outermost being the softest and most flexible ones. This indicates that the different teeth might experience different loads during foraging. With regard to the tested regions, we found that the bases and the bulges are most flexible and soft. This suggests that the teeth can bend in anterior-posterior direction around their bases, probably adjusting to the sizes of different prey items. Additionally, teeth are probably capable of bending in lateral-medial direction with the bulges serving as cushions (see Figure 8). This mechanical behaviour was also observed when the radula was manipulated by tweezers: the radula could be folded around the groove towards medial. As consequence the teeth bent towards the center forming a groove. SEM documentation revealed that the degree of wear and structural failure decreased towards the radular sides. All of this suggests, that during feeding, the Foraminifera (and the sand particles) or Porifera parts are clamped between the inner laterals during folding along the groove (Figure 8C). During this, the softer and more flexible outer teeth could serve as cushions and supporting structures, which would render this radula to be multifunctional since teeth have different functions. Subsequently, the radula with the particles or Porifera parts is pulled into the mouth cavity. This system would allow *G. rubrum* to take in all kind of different ingesta sizes, since its radula could easily adapt to prey shapes.

Besides the prey items, we detected various sand particles in the intestine. This indicates, that individuals of *G. rubrum* do not feed selectively, but instead probably feed on the sand surface and take everything randomly in. Since prey from the distal region of the intestine was more brittle and fractured than the prey extracted from the proximal regions, digestion in *G. rubrum* potentially involves acidic liquids.

Wear reduction

Wear reducing mechanisms are well-investigated in Polyplacophora and Patellogastropoda. Here, high proportion of Fe and Si are incorporated into a thick leading edge (surface layer), which is hard and protected against wear (Kirschvink & Lowenstam, 1979; Kim et al., 1989; Lowenstam & Weiner, 1989; van der Wal, 1989; van der Wal et al., 1999; Brooker et al., 2003; Lee et al., 2003a, 2003b; Saunders et al., 2009, 2011; Weaver et al., 2010; Wang et al., 2013; Kisailus & Nemoto, 2018; Krings et al., 2022c). Compared to the harder outer edge, the teeth possess a softer inner structure, which reduces crack formation (van der Wal, 1989; van der Wal et al., 1999; Grunfelder et al., 2014). In some paludomid and nudibranch taxa, we pre-

viously also identified an outer layer with high Si or Ca content on the tooth region, which interacts with the food (Krings et al., 2022a, 2023; Krings & Gorb, 2023a). This layer, however, was very thin in comparison with that of the chitons and limpets, rendering these teeth as lightweight structures. In *Gastropteron rubrum*, we detected high content of Si and Ca in the tooth regions, which interact with the ingesta. This suggests that this also reduces wear during feeding. A similar adaptation involving the incorporation of Si at the tooth tip and the presence of a soft tooth base to reduce wear by foraging on hard prey, such as diatoms, has also been found in the gnathobases of Copepoda (Michels et al., 2012).

The origin of the mechanical properties

In some taxa (i.e., Polyplacophora or Patellogastropoda), high proportions of inorganics, such as iron, silicon, and calcium, are incorporated into some tooth cusps which directly relate to mechanical property differences in the various tooth regions (for in depth reviews, see Brooker & Shaw, 2012; Faivre & Ukmar-Godec, 2015; Joester & Brooker, 2016). In *Gastropteron rubrum*, each tooth showed mechanical property gradients in its inner structure; but we could not relate these gradients with the inorganic content.

As the radula is composed of an organic matrix of chitin fibers with associated proteins (Runham, 1963; Guralnick & Smith, 1999), the fiber architecture (i.e., fiber density, size, etc.) can promote regional mechanical differences (Runham et al., 1963; van der Wal, 1989; Evans et al., 1990, 1994; van der Wal et al., 1999; Wealthall et al., 2005; Shaw et al., 2010; Gordon & Joester, 2011; Lu & Barber, 2012; Wang et al., 2013; Grunenfelder et al., 2014; Ukmar-Godec, 2016; Ukmar-Godec et al., 2017; Stegbauer et al., 2021; Krings et al., 2020, 2022a). Whether this is the case with *Gastropteron rubrum* awaits further investigations, e.g., in the form of tooth section investigations in TEM.

Chitin can also show different regional degrees of tanning, which result in different mechanical properties. The degree of tanning can be visualized by applying CLSM, applying the protocol of (Michels & Gorb, 2012). This protocol was developed for insect cuticle, which consists of unmineralized chitin. It allowed previously the identification of cuticle regions with certain dominating material composition: (a) Blue signals (i.e., autofluorescence signal produced by the laser of wavelength 405 nm) in cuticle was induced from regions containing high proportions of resilin or proteins; these regions were relatively soft and flexible. (b) Sclerotized cuticle was associated with a red signal (i.e., autofluorescence signal produced by the laser of wavelengths 555 and 639 nm); this region was relatively hard and stiff. (c) Weakly-sclerotized chitin with a green signal (i.e., autofluorescence signals produced by the laser of wavelength 488 nm) indicated regions which were flexible and relatively tough. When proteins were abundant, those structures appeared brown, yellow, or pink in overlay (i.e., showed strong autofluorescence signals produced by the laser of wavelengths 405 and 488 nm). This protocol (Michels & Gorb 2012) was applied in many studies on arthropod cuticles (e.g., Peisker et al., 2013; Friedrich & Kubiak, 2018; Beutel et al., 2020, Matsumura et al., 2021; Lehnert et al., 2021) and cross-validated by employing nanoindentation in lady beetles and antlions (Peisker et al., 2013; Krings & Gorb, 2023b).

The same protocol was applied for the first time bei Krings et al. (2022d) to the radula of the paludomid *Lavigeria grandis*, which possesses relatively low mineral content. Here, the autofluorescence signals directly related to the mechanical property values received from nanoindentation technique. We also applied this protocol for the radulae of the nudibranch gastropods *Felimare picta* and *Doris pseudoargus*, but detected that the autofluorescence signal was distorted by the content of Ca and Si in the tooth surfaces (Krings et al., 2023). Nudibranch teeth with surfaces full of Ca showed a strong blue signal (i.e., autofluorescence signal produced by the laser of wavelength 405 nm), and teeth containing high Si content in the surfaces a strong green signal (i.e., autofluorescence signal produced by the laser of wavelength 488 nm). This pattern was previously also detected in crustacean feeding structures, the gnathobases and gastric mill teeth, containing either high content of Ca or Si (Michels et al., 2012; Michels & Gorb, 2012; Krings et al., 2022b). In *G. rubrum*, we detected that the surfaces containing Si appeared green (i.e., showed a strong autofluorescence signal after excitement by the laser of wavelength 488 nm). This shows that the protocol of Michels & Gorb (2012) cannot be directly applied to mineralized structures and that EDX analyses should be included into studies. However, the tooth sides of *G. rubrum* did not contain high proportions of Ca and Si, so that the

protocol can be applied to these regions. The results indicate, that the teeth are probably sclerotized with a decreasing degree towards the basis. The bases and bulges of *G. rubrum* teeth were unmineralized and appeared blue (i.e., showed a strong autofluorescence signal after excitement by the laser of wavelength 405 nm), which indicates that less crosslinked organic materials are abundant in these regions, which probably increase both the softness and flexibility of material.

Declarations

Ethics approval and consent to participate. Not applicable.

Consent for publication. Not applicable

Data Accessibility Statement. The 3D model will be deposited in Dryad. The data on mechanical properties and elemental analysis can be found in the Supplementary.

Competing interests. The authors declare that they have no competing interests

Funding. This research was financed by the DFG grant KR 5540/2-1 to WK.

Authors' contributions. WK, SG, and HW initiated the study. WK performed nanoindentation, WK and CN performed SEM and EDX analyses. WK wrote the first draft of the manuscript. AK modelled the radular teeth. All authors contributed to and approved the final version of the manuscript for publication.

Acknowledgements. We would like to thank Elke Woelken from the Institute of Cell and Systems Biology of Animals, Universität Hamburg, for their support on the SEM. We are highly grateful for the helpful comments of the anonymous reviewers.

References

- Anderson, P.S.L., 2018. Making a point: shared mechanics underlying the diversity of biological puncture. *J. Exp. Biol.* 221, jeb187294.
- Barber, A.H., Lu, D., Pugno, N.M., 2015. Extreme strength observed in limpet teeth. *J. Royal Soc. Interface* 12(105), 20141326.
- Bendsoe, M.P., 1989. Optimal shape design as a material distribution problem. *Struct. Optim.* 1, 193–202.
- Bendsoe, M.P., 1995. Optimization of structural topology. *Shape and material*. Springer, Berlin.
- Bendsoe, M.P., Kikuchi, N., 1988. Generating optimal topologies in structural design using a homogenization method. *Comput. Methods Appl. Mech. Eng.* 71, 197–224.
- Beutel, R.G., Richter, A., Keller, R.A., Garcia, F.H., Matsumura, Y., Economo, E.P., Gorb, S.N., 2020. Distal leg structures of the Aculeata (Hymenoptera): A comparative evolutionary study of *Sceliphron* (Sphecidae) and *Formica* (Formicidae). *J. Morphol.* 281, 737–753.
- Brooker, L.R., Lee, A.P., Macey, D.J., van Bronswijk, W., Webb, J., 2003. Multiple-front iron-mineralisation in chiton teeth (*Acanthopleura echinata*: Mollusca: Polyplacophora). *Mar. Biol.* 142, 447–454.
- Brooker, L.R., Shaw, J.A., 2012. The chiton radula: A unique model for biomineralization studies. In: Seto, J., editor. *Advanced topics in biomineralization*. Rijeka, Croatia, Intech Open, pp. 65–84.
- DeLaHoz, M.V., Sarda, F., Coll, M., Saez, R., Mecho, A., Oliva, F., Ballesteros, M., Palomera, I., 2018. Biodiversity patterns of megabenthic non-crustacean invertebrates from an exploited ecosystem of the north-western Mediterranean Sea. *Reg. Stud. Mar. Sci.* 19, 47–68.
- Dumont, E.R., Grosse, I.R., Slater, G.J., 2009. Requirements for comparing the performance of finite element models of biological structures. *J. Theor. Biol.* 256, 96–103.
- Evans, L.A., Macey, D.J., Webb, J., 1990. Characterization and structural organization of the organic matrix of radula teeth of the chiton *Acanthopleura hirtosa*. *Phil. Trans. R. Soc. Lond. B* 329, 87–96.

- Evans, L.A., Macey, D.J., Webb, J., 1994. Matrix heterogeneity in the radular teeth of the chiton *Acanthopleura hirtosa*. *Acta Zool.* 75, 75–79.
- Faivre, D., Ukmar-Godec, T., 2015. From bacteria to mollusks: The principles underlying the biomineralization of iron oxide materials. *Angew. Chem. Int. Ed.* 54(16), 4728–4747.
- Freeman, P.W., Lemen, C.A., 2007. The trade-off between tooth strength and tooth penetration: predicting optimal shape of canine teeth. *J. Zool.* 273, 273–280.
- Friedrich, F., Kubiak, M., 2018. Comparative anatomy of pupal tarsi in caddisflies (Insecta: Trichoptera) with focus on the claw system. *Zoomorphology* 137, 305–314.
- Gorb, S.N., Krings, W., 2021. Mechanical property gradients of taenioglossan radular teeth are associated with specific function and ecological niche in Paludomidae (Gastropoda: Mollusca). *Acta Biomater.* 134(15), 513–530.
- Gordon, L., Joester, D., 2011. Nanoscale chemical tomography of buried organic – inorganic interfaces in the chiton tooth. *Nature* 469, 194–198.
- Grunenfelder, L.K., de Obaldia, E.E., Wang, Q., Li, D., Weden, B., Salinas, C., Wuhner, R., Zavattieri, P., Kisailus, D., 2014. Biomineralization: stress and damage mitigation from oriented nanostructures within the radular teeth of *Cryptochiton stelleri*. *Adv Funct Mater* 24(39), 6093–6104.
- Guralnick, R., Smith, K., 1999. Historical and biomechanical analysis of integration and dissociation in molluscan feeding, with special emphasis on the true limpets (Patellogastropoda: Gastropoda). *J. Morphol.* 241, 175–195.
- Han, Y., Liu, C., Zhou, D., Li, F., Wang, Y., Han, X., 2011. Magnetic and structural properties of magnetite in radular teeth of chiton *Acanthochiton rubrolinestus*. *Bioelectromagnetics* 32, 226–233.
- Hawkins, S.J., Watson, D.C., Hill, A.S., Harding, S.P., Kyriakides, M.A., Hutchinson, S., Norton, T.A., 1989. A comparison of feeding mechanisms in microphagous, herbivorous, intertidal, prosobranchs in relation to resource partitioning. *J. Molluscan Stud.* 55(2), 151–165.
- Herrera, S.A., Grunenfelder, L., Escobar, E., Wang, Q., Salinas, C., Yaraghi, N., Geiger, J., Wuhner, R., Zavattieri, P., Kisailus, D., 2015. Stylus support structure and function of radular teeth in *Cryptochiton stelleri*. 20th International Conference on Composite Materials, Copenhagen, 19–24th July.
- Hickman, C.S., 1980. Gastropod radulae and the assessment of form in evolutionary paleontology. *Paleobiology* 6, 276–294.
- Hickman, C.S., 1984. Implications of radular tooth-row functional-integration for archaeogastropod systematics. *Malacologia* 25, 143–160.
- Joester, D., Brooker, L.R., 2016. The chiton radula: A model system for versatile use of iron oxides. In: Faivre, D., editor. *Iron oxides: From nature to applications*. Weinheim: Wiley-VCH, p. 177–205.
- Kim, K.S., Macey, D.J., Webb, J., Mann, S., 1989. Iron mineralisation in the radula teeth of the chiton *Acanthopleura hirtosa*. *Proc. Royal Soc. B* 237, 335–346.
- Kirschvink, J.L., Lowenstam, H.A., 1979. Mineralization and magnetization of chiton teeth: paleomagnetic, sedimentologic and biologic implications of organic magnetite. *EPSL* 44(2), 193–204.
- Kisailus, D., Nemoto, M., 2018. Structural and proteomic analyses of iron oxide biomineralization in chiton teeth. In: Matsunaga T, Tanaka T, Kisailus D, editors. *Biological magnetic materials and applications*. Singapore, Springer, pp. 53–73.
- Krings, W., 2020. Trophic specialization of paludomid gastropods from 'ancient' Lake Tanganyika reflected by radular tooth morphologies and material properties. Dissertation, University of Hamburg.

- Krings, W., Brutt, J.-O., Gorb, S.N., 2022a. Micro-cracks and micro-fractures reveal radular tooth architecture and its functional significance in the paludomid gastropod *Lavigeria grandis* . *Philos. Trans. Royal Soc. A* 380, 20210335.
- Krings, W., Brutt, J.-O., Gorb, S.N., 2022b. Mechanical properties, degree of sclerotisation and elemental composition of the gastric mill in the red swamp crayfish *Procambarus clarkii* (Decapoda, Crustacea). *Sci. Rep.* 12, 17799.
- Krings, W., Brutt, J.-O., Gorb, S.N., 2022c. Ontogeny of the elemental composition and the biomechanics of radular teeth in the chiton *Lepidochitona cinerea* . *Front. Zool.* 19, 19.
- Krings, W., Brutt, J.-O., Gorb, S.N., 2022d. Material gradients in gastropod radulae and their biomechanical significance: a combined approach on the paludomid *Lavigeria grandis* . *Sci. Nat.* 109, 52.
- Krings, W., Brutt, J.-O., Gorb, S.N., Glaubrecht, M., 2020. Tightening it up: diversity of the chitin anchorage of radular-teeth in paludomid freshwater-gastropods. *Malacologia* 63, 77–94.
- Krings, W., Gorb, S.N., 2021. Radula packing and storage facilitated by tooth morphology in selected taenioglossan Gastropoda. *J. Molluscan Stud.* 87, eyab007.
- Krings, W., Gorb, S.N., 2023a. Resistance to abrasive particles in soft radular teeth (Paludomidae, Gastropoda, Mollusca). Under review at *Invertebrate Biology*.
- Krings, W., Gorb, S.N., 2023b Mechanical properties of larval mouthparts of the antlion *Euroleon nostras* (Neuroptera: Myrmeleontidae) and their correlation with cuticular material composition. Under review at *Zoomorphology*.
- Krings, W., Karabacak, H., Gorb, S.N., 2021d. From the knitting shop: The first physical and dynamic model of the taenioglossan radula (Mollusca: Gastropoda) aids in unravelling functional principles of the radular morphology. *J. Royal Soc. Interface* 18(182), 20210377.
- Krings, W., Kovalev, A., Glaubrecht, M., Gorb, S.N., 2019. Differences in the Young modulus and hardness reflect different functions of teeth within the taenioglossan radula of gastropods. *Zoology* 137, 125713.
- Krings, W., Kovalev, A., Gorb, S.N., 2021b. Influence of water content on mechanical behaviour of gastropod taenioglossan radulae. *Proc. Royal Soc. B* 288, 20203173.
- Krings, W., Kovalev, A., Gorb, S.N., 2021c. Collective effect of damage prevention in taenioglossan radular teeth is related to the ecological niche in Paludomidae (Gastropoda: Cerithioidea). *Acta Biomater.* 135, 458–172.
- Krings, W., Marce-Nogue, J., Gorb, S.N., 2021e. Finite element analysis relating shape, material properties, and dimensions of taenioglossan radular teeth with trophic specialisations in Paludomidae (Gastropoda). *Sci. Rep.* 11, 22775.
- Krings, W., Marce-Nogue, J., Karabacak, H., Glaubrecht, M., Gorb, S.N., 2020. Finite element analysis of individual taenioglossan radular teeth (Mollusca). *Acta Biomater.* 115, 317–332.
- Krings, W., Wagele, H., Neumann, C., Gorb, S.N., 2023. Coping with abrasive ingesta – diverging composition of radular teeth in two Porifera-consuming nudibranch species (Mollusca, Gastropoda). Under review at *Journal of the Royal Society Interface*.
- Lee, A.P., Brooker, L.R., Macey, D.J., Webb, J., van Bronswijk, W., 2003a. A new biomineral identified in the cores of teeth from the chiton *Plaxiphora albida* . *J. Biol. Inorg. Chem.* 8, 256–262.
- Lee, A.P., Brooker, L.R., van Bronswijk, W., Macey, D.J., Webb, J., 2003b. Contribution of Raman spectroscopy to identification of biominerals present in teeth of *Acanthopleura rehderi* , *Acanthopleura curtisiana* , and *Onithochiton quercinus* . *Biopolymers* 72, 299–301.

- Lehnert, M.S., Johnson, D.D., Wu, J., Sun, Y., Fonseca, R.J., Michels, J., Shell, J.S., Reiter, K.E., 2021. Physical adaptations of butterfly proboscises enable feeding from narrow floral tubes. *Funct. Ecol.* 35, 1925–1937.
- Lowenstam, H.A., Weiner, S., 1989. Mollusca. In: Lowenstam HA, Weiner S, editors. *On biomineralization*. Oxford, Oxford University Press, pp. 88–305.
- Lu, D., Barber, A.H., 2012. Optimized nanoscale composite behaviour in limpet teeth. *J. Royal Soc. Interface* 9(71), 1318–1324.
- Mackenstedt, U., Markel, K., 1987. Experimental and comparative morphology of radula renewal in pulmonates (Mollusca, Gastropoda). *Zoomorphology* 107, 209–239.
- Matsumura, Y., Kovalev, A., Gorb, S.N., 2021. Mechanical properties of a female reproductive tract of a beetle and implications for penile penetration. *Proc. Royal Soc. B.* 288, 20211125.
- Michels, J., Gorb, S.N., 2012. Detailed three-dimensional visualization of resilin in the exoskeleton of arthropods using confocal laser scanning microscopy. *J. Microsc.* 245(1), 1–16.
- Michels, J., Gorb, S.N., 2015. Mandibular gnathobases of marine planktonic copepods — Structural and mechanical challenges for diatom frustules in evolution of lightweight structures. In: Hamm, C., editor. *Biologically-inspired systems*. Dordrecht, Springer, pp. 59–73.
- Michels, J., Vogt, J., Gorb, S.N., 2012. Tools for crushing diatoms – opal teeth in copepods feature a rubber-like bearing composed of resilin. *Sci. Rep.* 2, 465.
- Montroni, D., Zhang, X., Leonard, J., Kaya, M., Amemiya, C., Falini, G., Rolandi, M., 2019. Structural characterization of the buccal mass of *Ariolimax californicus* (Gastropoda; Stylommatophora). *PLoS One* 14, e0212249.
- Morris, T.E., Hickman, C.S., 1981. A method for artificially protruding gastropod radulae and a new model of radula function. *Veliger* 24, 85–89.
- Morrow, C., Cardenas, P., 2015. Proposal for a revised classification of the Demospongiae (Porifera). *Front. Zool.* 12, 7.
- Ong, E., Hallas, J.M., Gosliner, T.M., 2017. Like a bat out of heaven: the phylogeny and diversity of the bat-winged slugs (Heterobranchia: Gastropteridae). *Zool. J. Linn. Soc.* 180(4), 755–789.
- Padilla, D.K., 2003. Form and function of radular teeth of herbivorous molluscs: Focus on the future. *Am. Malacol. Bull.* 18(1-2), 163–168.
- Peisker, H., Michels, J., Gorb, S.N., 2013. Evidence for a material gradient in the adhesive tarsal setae of the ladybird beetle *Coccinella septempunctata*. *Nat. Commun.* 4, 1661.
- Pohl, A., Herrera, S.A., Restrepo, D., Negishi, R., Jung, J.-Y., Salinas, C., Wuhler, R., Yoshino, T., McKittrick, J., Arakaki, A., Nemoto, M., Zavattieri, P., Kisailus, D., 2020. Radular stylus of *Cryptochiton stelleri*: A multifunctional lightweight and flexible fiber-reinforced composite. *J. Mech. Behav. Biomed. Mater.* 111, 103991.
- Runham, N.W., 1963. A study of the replacement mechanism of the pulmonate radula. *J. Cell. Sci.* 3(66), 271–277.
- Runham, N.W., Isarankura, K., 1966. Studies on radula replacement. *Malacologia* 5, 73.
- Saunders, M., Kong, C., Shaw, J.A., Clode, P.L., 2011. Matrix-mediated biomineralization in marine mollusks: A combined transmission electron microscopy and focused ion beam approach. *Microsc. Microanal.* 17, 220–225.

- Saunders, M., Kong, C., Shaw, J.A., Macey, D.J., Clode, P.L., 2009. Characterization of biominerals in the radula teeth of the chiton, *Acanthopleura hirtosa*. J. Struct. Biol. 167, 55–61.
- Shaw, J.A., Macey, D.J., Brooker, L.R., Clode, P.L., 2010. Tooth use and wear in three iron-biomineralizing mollusc species. Biol. Bull. 218, 132–144.
- Shaw, J.A., Macey, D.J., Brooker, L.R., Stockdale, E.J., Saunders, M., Clode, P.L., 2009a. The chiton stylus canal: An element delivery pathway for tooth cusp biomineralization. J. Morphol. 270, 588–600.
- Shaw, J.A., Macey, D.J., Brooker, L.R., Stockdale, E.J., Saunders, M., Clode, P.L., 2009b. Ultrastructure of the epithelial cells associated with tooth biomineralization in the chiton *Acanthopleura hirtosa*. Microsc. Microanal. 15(2), 154–165.
- Solem, A., 1972. Malacological applications of scanning electron microscopy II. Radular structure and functioning. Veliger 14, 327–336.
- Solem, A., 1974. The shell makers: Introducing mollusks. New York, Jon Wiley & Sons.
- Stegbauer, L., Smeets, P.J.M., Free, R., Wallace, S.G., Hersam, M.C., Alp, E.E., Joester, D., 2021. Persistent polymorphism in the chiton tooth: from a new biomineral to inks for additive manufacturing. Proc. Natl. Acad. Sci. USA 118, e2020160118.
- Steneck, R.S., Watling, L., 1982. Feeding capabilities and limitation of herbivorous molluscs: A functional group approach. Mar. Biol. 68, 299–319.
- Ukmar-Godec, T., 2016. Mineralization of goethite in limpet radular teeth. In: Faivre D, editor. Iron oxides: from nature to applications. Weinheim, Wiley-VCH, pp. 207–224.
- Ukmar-Godec, T., Bertinetti, L., Dunlop, J.W.C., Godec, A., Grabiger, M.A., Masic, A., Nguyen, H., Zlotnikov, I., Zaslansky, P., Faivre, D., 2017. Materials nanoarchitecturing via cation-mediated protein assembly: making limpet teeth without mineral. Adv. Mater. 29(27), 1701171.
- Ukmar-Godec, T., Kapun, G., Zaslansky, P., Faivre, D., 2015. The giant keyhole limpet radular teeth: A naturally-grown harvest machine. J. Struct. Biol. 192, 392–402.
- van der Wal, P., 1989. Structural and material design of mature mineralized radula teeth of *Patella vulgata* (Gastropoda). J. Ultrastruct. Mol. Struct. Res. 102, 147–161.
- van der Wal, P., Giesen, H.J., Videler, J.J., 1999. Radular teeth as models for the improvement of industrial cutting devices. Mater. Sci. Eng. C 7(2), 129–142.
- van der Wal, P., Videler, J.J., Havinga, P., Pel, R., 1989. Architecture and chemical composition of the magnetite-bearing layer in the radula teeth of *Chiton olivaceus* (Polyplacophora). In: Crick, R.E., editor. Origin, evolution, and modern aspects of biomineralization in plants and animals. Boston, MA, Springer, pp. 153–166.
- Vortsepneva, E., Mikhлина, A., Kantor, Y., 2022. Main patterns of radula formation and ontogeny in Gastropoda. J. Morphol. Accepted Author Manuscript. <https://doi.org/10.1002/jmor.21538>
- Wang, C., Li, Q.Y., Wang, S.N., Qu, S.X., Wang, X.X., 2014. Microstructure and self-sharpening of the magnetite cap in chiton tooth. Mater. Sci. Eng. C 37, 1–8.
- Wang, Q., Nemoto, M., Li, D., Weaver, J.C., Weden, B., Stegemeier, J., Bozhilov, K.N., Wood, L.R., Milliron, G.W., Kim, C.S., DiMasi, E., Kisailus, D., 2013. Phase transformations and structural developments in the radular teeth of *Cryptochiton stelleri*. Adv. Funct. Mater. 23, 2908–2917.
- Wealthall, R.J., Brooker, L.R., Macey, D.J., Griffin, B.J., 2005. Fine structure of the mineralized teeth of the chiton *Acanthopleura echinata* (Mollusca: Polyplacophora). J. Morphol. 265, 165–175.

Weaver, J.C., Wang, Q., Miserez, A., Tantuccio, A., Stromberg, R., Bozhilov, K.N., Maxwell, P., Nay, R., Heier, S.T., DiMasi, E., 2010. Analysis of an ultra hard magnetic biomineral in chiton radular teeth. *Mater. Today* 13(1–2), 42–52.

Figures and legends

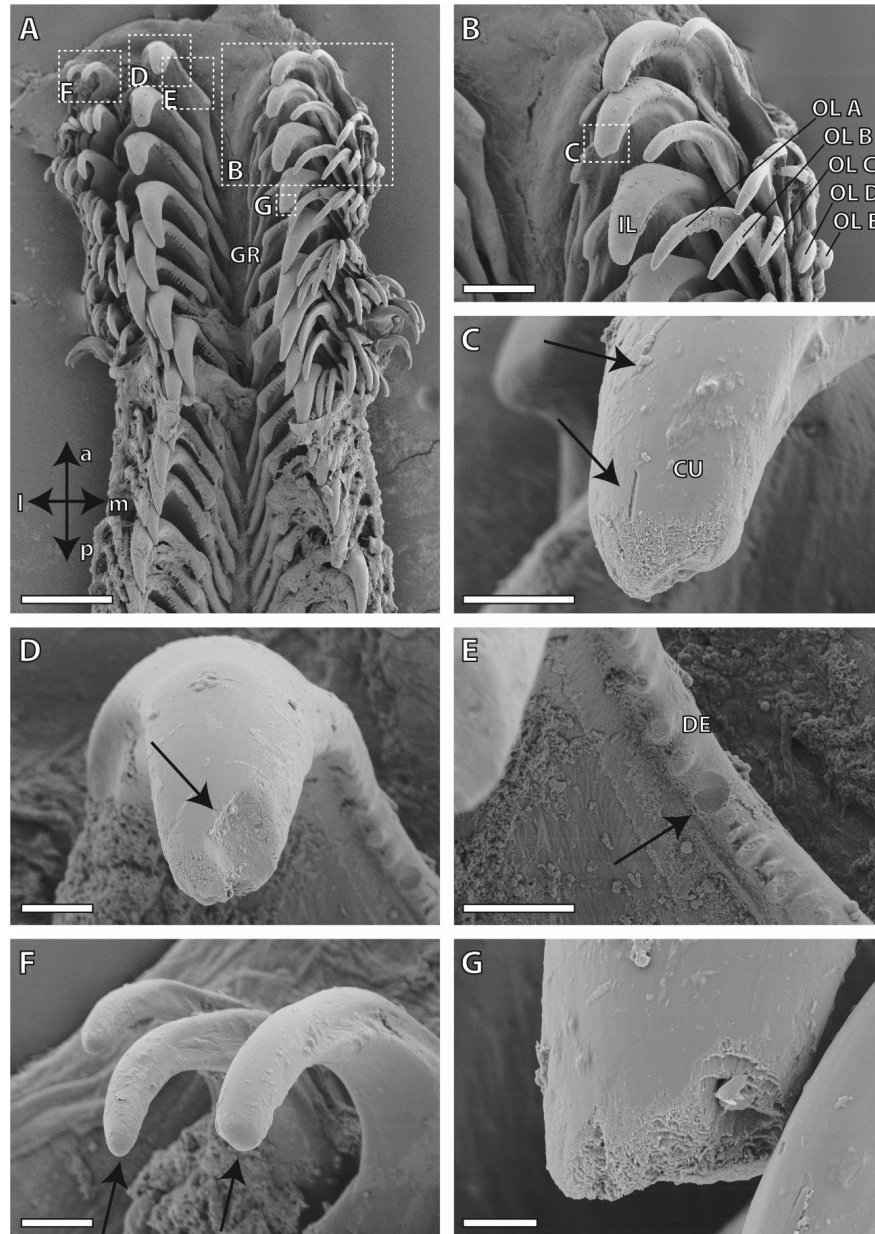


Figure 1. A. Radula, overview with anatomical directions. B–G. Magnifications, displaying cracks and wear (highlighted by arrows), probably resulting from interaction with hard ingesta particles (stones, spicules, Foraminifera tests). Abbreviations: a, anterior (towards the degenerative zone); CU, cusp; DE, denticle; GR, groove; IL, inner lateral; l, lateral; m, medial; OL A, outer lateral A; OL B, outer lateral B; OL C, outer lateral C; OL D, outer lateral D; OL E, outer lateral E; p, posterior (towards the building zone). Scale bars: A, 200 μm ; B, 80 μm ; C, D, E, F, 20 μm ; G, 8 μm .

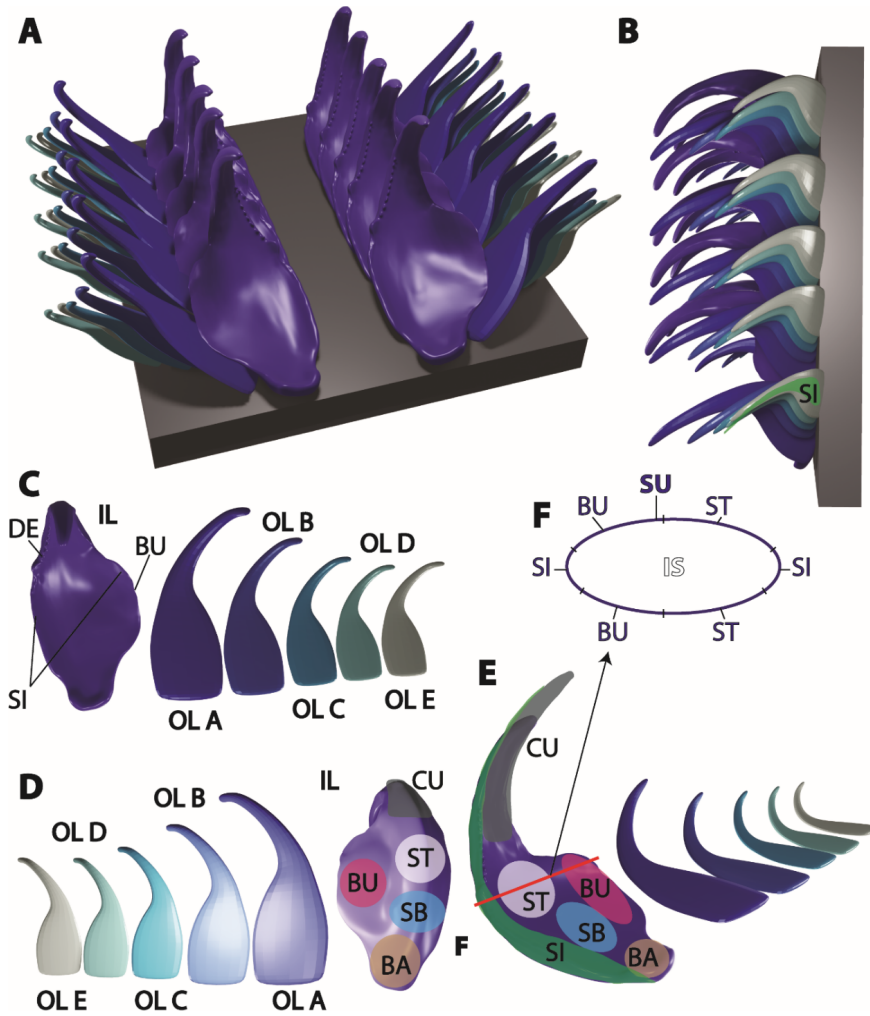


Figure 2. 3D model of the radula to introduce the nomenclature of tooth regions and the sites that were tested. A. Radula from above. B. Radula from the side. C. The individual teeth from above. D. From below. E. Teeth from medial view, the red line indicates a cross section, from where point-measurements were taken via EDX. F. Schematic outline of a characteristic polished section area of a tooth. When this area was on display, the inner structure and the surfaces could be tested with point-measurements via EDX. The surface was separated into different regions (surface of e.g., the bulge, the stylus, the sides). Abbreviations: BA, basis; BU, bulge; CU, cusp; DE, denticle; IL, inner lateral; IS, inner structure; OL A, outer lateral A; OL B, outer lateral B; OL C, outer lateral C; OL D, outer lateral D; OL E, outer lateral E; SB, basis of stylus; SI, side; ST, terminal stylus; SU, surface.

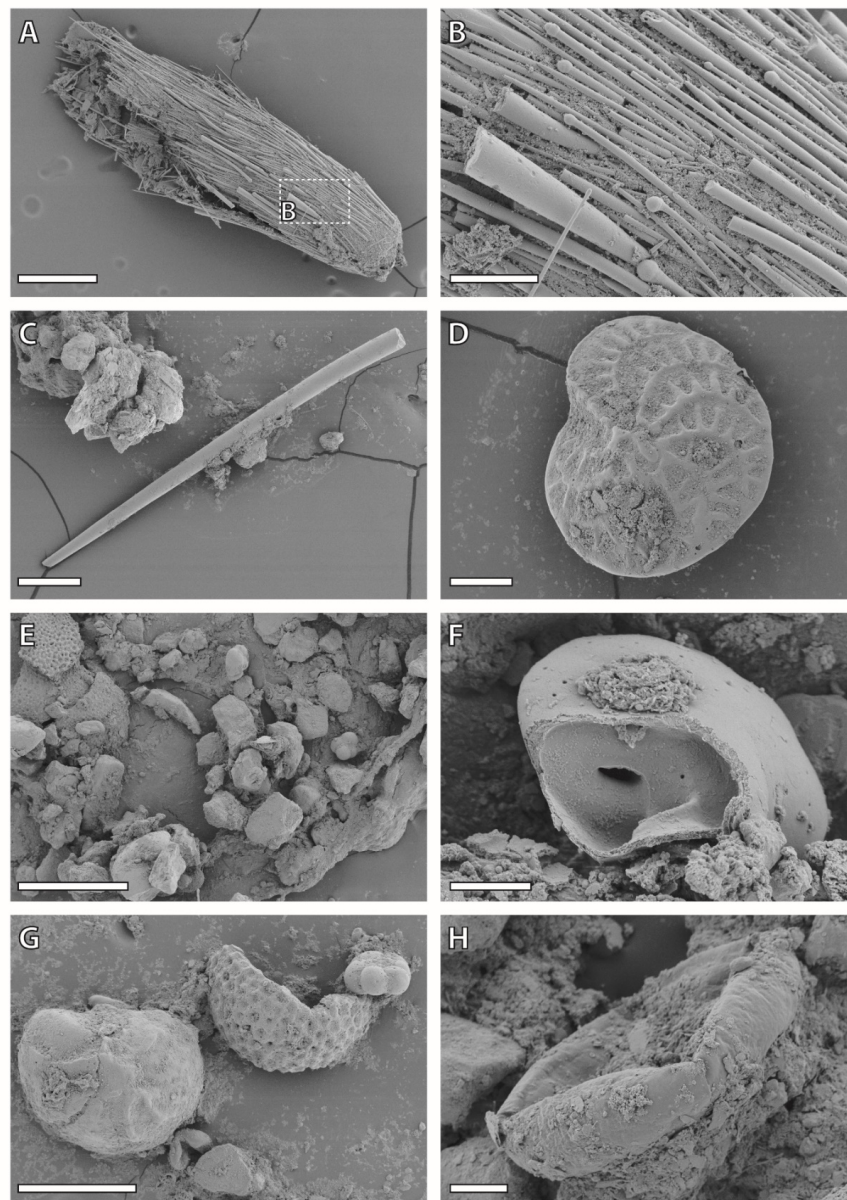


Figure 3. Intestine content. A–C. Spiculae, including from tylostyle type, indicating their origin from Heteroscleromorpha (Porifera). D. Foraminifera, extracted from the proximal region of the intestine. E. Intestine content with tests of Foraminifera and stones. F. Cracked Foraminifera tests. G. Foraminifera from the distal region of the intestine. H. Diatom. Scale bars: A, 400 μm ; B, D, 80 μm ; C, G, 200 μm ; E, 400 μm ; F, 20 μm ; H, 40 μm .

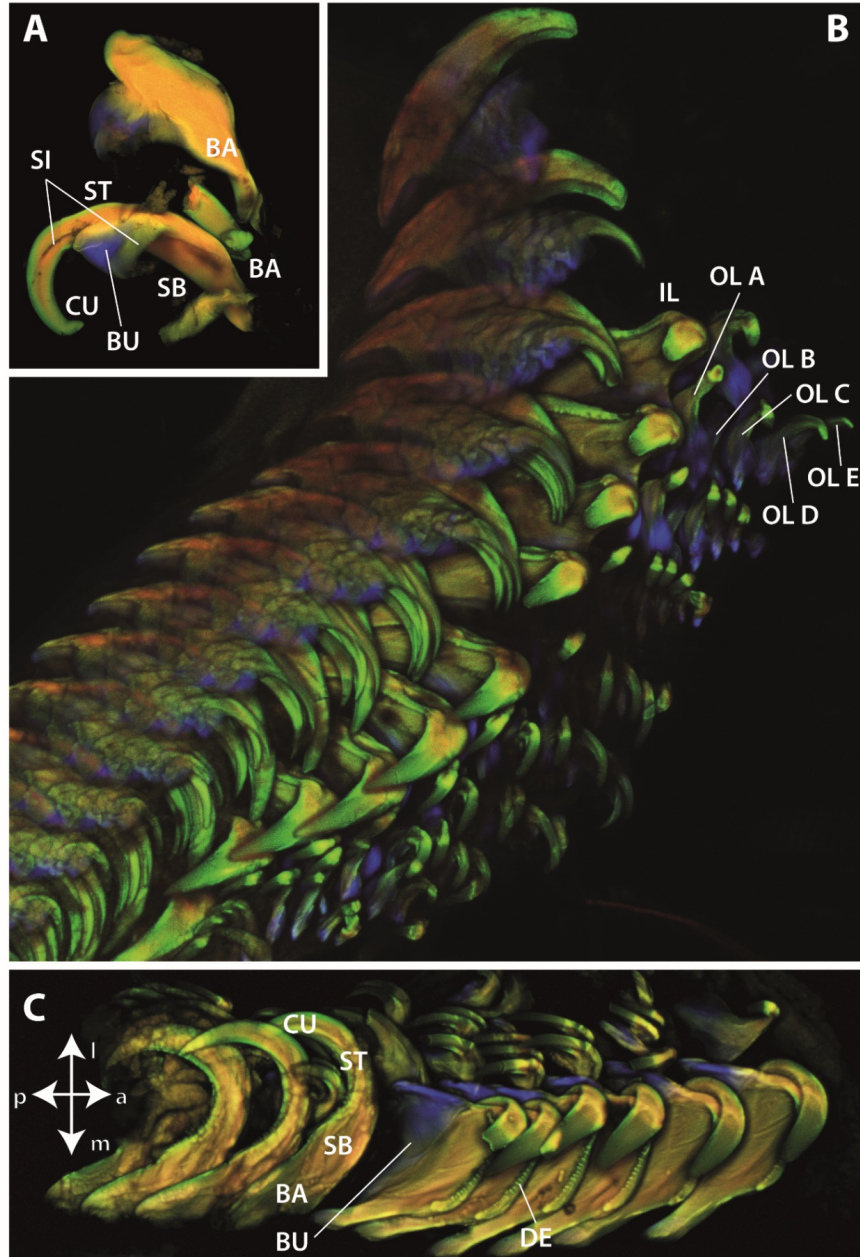


Figure 4. CLSM images of *Gastroteron rubrum* radula. A. Mature inner lateral teeth. B. Whole radula. C. One side of the radular working zone. Abbreviations: a, anterior (towards the degenerative zone); BA, basis; BU, bulge; CU, cusp; DE, denticle; IL, inner lateral; l, lateral; m, medial; OL A, outer lateral A; OL B, outer lateral B; OL C, outer lateral C; OL D, outer lateral D; OL E, outer lateral E; p, posterior (towards the building zone); SB, basis of stylus; SI, side; ST, terminal stylus.

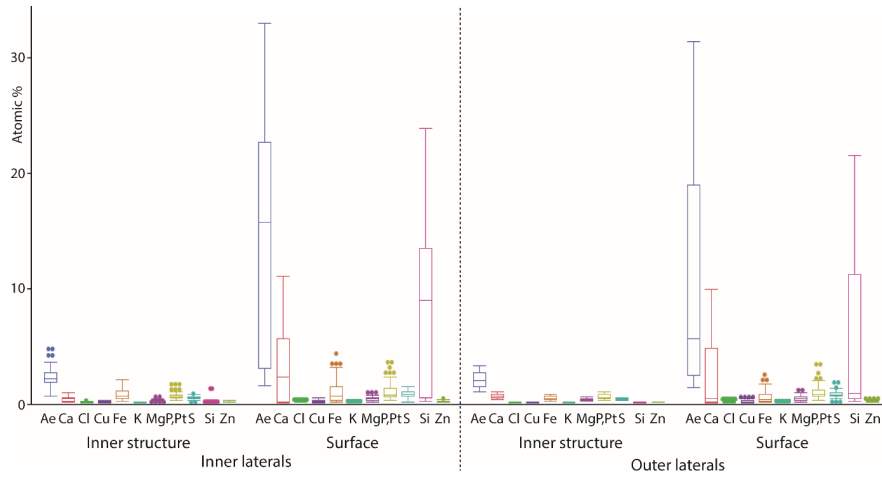


Figure 5. Results from the EDX analysis. Content of Ca, Cl, Cu, Fe, K, Mg, P+Pt, S, Si, Zn and Ae (sum of Ca, Cl, Cu, Fe, K, Mg, P+Pt, S, Si, and Zn) for the inner tooth structure and the tooth surface (all tooth types and regions are pooled together).

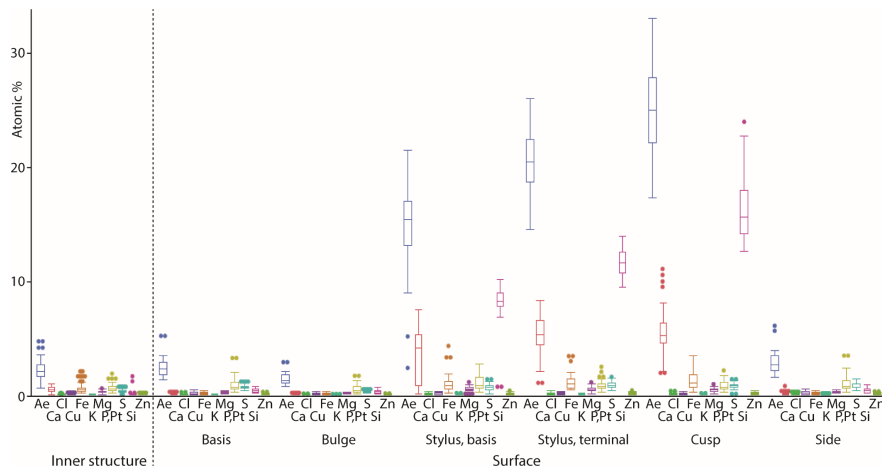


Figure 6. Results from the EDX analysis. Contents of Ca, Cl, Cu, Fe, K, Mg, P+Pt, S, Si, Zn and Ae (sum of Ca, Cl, Cu, Fe, K, Mg, P+Pt, S, Si, and Zn) for the inner tooth structure and the tooth surface regions (tooth types are pooled together).

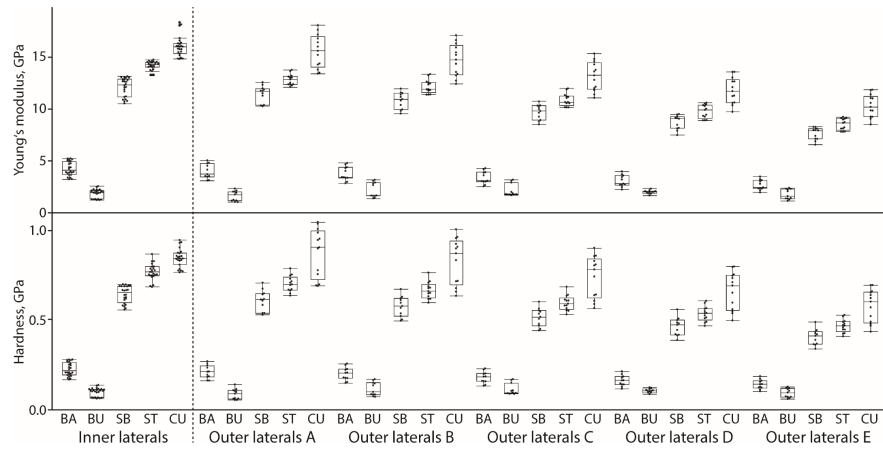


Figure 7. Results from the nanoindentation experiments. Young's modulus and hardness (both given in GPa) for the different teeth and their regions. BA, basis; BU, bulge; CU, cusp; SB, basis of stylus; ST, terminal stylus.

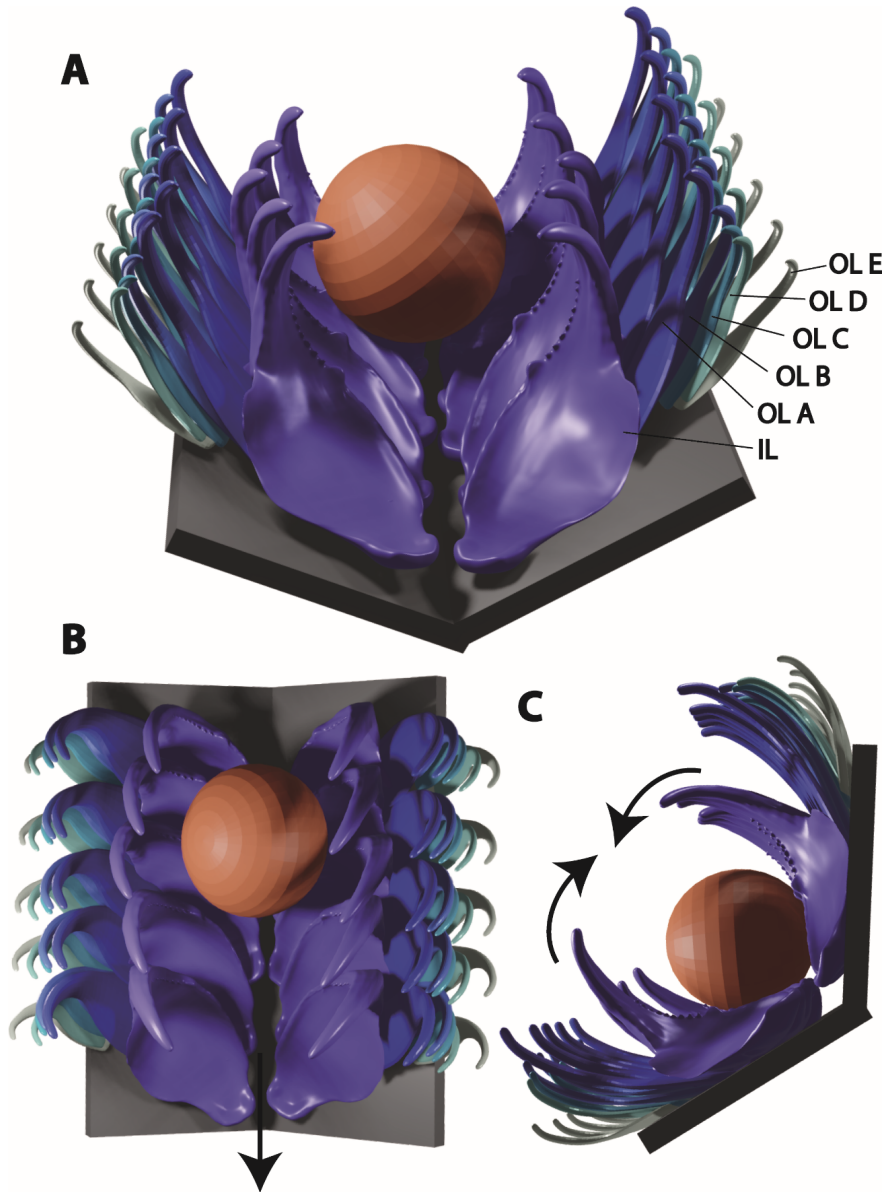


Figure 8. Proposed biomechanical behaviour of *Gastropteron* radula, based on mechanical property tests and the documentation of the radular wear. A. Radula 3D model from frontal view with clamped Foraminifera between inner laterals. B. Model from above. C. Model from the side. Arrows indicate the folding towards the radular groove, which enables the clamping of ingesta. Afterwards the radula with the particles is pulled into the mouth cavity (arrow in B).